Synthesis and properties of a magnetic core–shell composite nano-adsorbent for fluoride removal from drinking water

Chang Zhang, Lin Chen, Ting-Jie Wang*, Chao-Li Su, Yong Jin

Department of Chemical Engineering, Tsinghua University, 100084 Beijing, China

ARTICLE INFO

ABSTRACT

An adsorbent for fluoride removal from drinking water was prepared by coating Fe–Ti bimetallic oxide on magnetic Fe_3O_4 particles by co-precipitation. The adsorbent was a nanosized composite with a core–shell structure comprising a magnetic Fe_3O_4 core of 10–20 nm in diameter and an amorphous adsorbent shell of several nanometer thickness. The synthesis parameters were optimized to give high adsorption capacity and high magnetization. The optimized mass ratio of the Fe–Ti bimetallic oxide shell to Fe_3O_4 core was 2.72. The adsorption isotherm was well fitted with the Langmuir isotherm and the saturation adsorption capacity 57.22 mg/g adsorbent. Adsorption was fast and reached equilibrium within 2 min. The nano-adsorbent was superparamagnetic with a saturation magnetization of 18.4 emu/g, which allowed rapid separation of the adsorbent from the water solution by an external magnet.

1. Introduction

Excess fluoride uptake can cause mottled teeth, brittle bones, and even damage to neurological and reproductive systems [1,2]. A fluoride concentration below 1.5 mg/L in drinking water is recommended by the World Health Organization (WHO) [3], and a maximum of 1.0 mg/L is required by Chinese drinking water standards (GB5749-2006). The weathering and leaching of fluorinated minerals, and industrial wastewater discharges are the main sources of fluoride in groundwater. With increased human industrial activities, high fluoride-content water has become a widespread problem in the world [4,5].

Various methods [4–12] have been used to remove excess fluoride from water, which include adsorption [6–8], ion exchange [9], precipitation and flocculation [10], membrane separation [11], electrodialysis and electrolysis [12]. Adsorption is the most widely used method due to its simplicity, low cost, and high efficiency. Many high adsorption capacity adsorbents have been developed. A metal oxide nano-adsorbent is one of the most effective adsorbents for fluoride removal due to its large specific surface area, high adsorption capacity and adsorption rate [4,5,13–18]. In our previous work [13,14], a novel iron-titanium (Fe–Ti) oxide adsorbent

was prepared. The Fe–Ti oxide has higher adsorption capacities than other Fe-based adsorbent, as shown in Table 1, and has low cost due to its iron component. However, the use of a nano-adsorbent in practical applications is very difficult because adsorption in a packed bed is commonly used for fluoride removal, but a nano-sized adsorbent will cause a huge pressure drop in a packed bed due to its extremely small size. A solution is to disperse the nano-adsorbent in a fluidized system, but then the separation of the nano-adsorbent from the water solution is a problem to be solved [19,20].

Magnetic separation provides a promising way to perform solid–liquid separation of the nano-adsorbent and water. In recent years, magnetic composite particles have been widely studied for this. The magnetic component of the composite particles is commonly superparamagnetic Fe_3O_4. In the absence of an external magnetic field, the superparamagnetic particles can be well dispersed in water. After adsorption, the composite particles can be collected easily by a magnet, and re-dispersed in water without undesired magnetic aggregation when the magnet is removed. Magnetic particles loaded with various functional components are used in many fields such as targeted drug delivery [21], protein separation [22], photo-catalyst separation [23,24], hazardous substances adsorption [25,26], etc. So far, there are some reports in the literature on the use of non-magnetic adsorbents combined with magnetic particles to give high adsorption capacity and easy separation [19,20,27–29], but the detailed structure of the composite particles, nano-particle residues resulting from incomplete

* Corresponding author at: Department of Chemical Engineering, Tsinghua University, 100084 Beijing, China. Tel.: +86 10 62788993; fax: +86 10 62772051.
E-mail address: wangtj@tsinghua.edu.cn (T.-J. Wang).

Table 1
Adsorption capacities of Fe–Ti oxide adsorbent and other iron-based adsorbent.

Adsorbents	Fe–Ti [14]	Fe–Al [15]	Fe–Zr [16]	Fe–Sn [17]	Fe–Cr [18]
Q_{max} (mg/g)	53.22	17.7	8.2	10.5	16.3

solid–liquid separation, and water contamination caused by adsorbent dissolution or abrasion were not studied, even though these issues are very important in practical application.

In this paper, a novel composite adsorbent with a core–shell structure was prepared for efficient removal of fluoride in drinking water by coating the excellent nano-adsorbent of iron-titanium (Fe–Ti) oxide onto magnetic Fe_3O_4 particles. The core–shell structure of the composite particles was examined and analyzed. The adsorption capacity and adsorption rate were studied. The separation efficiency and residues were measured and discussed.

2. Materials and methods

2.1. Material

$FeCl_3·6H_2O$ (Sinopharm Chemical Reagent Company) and $FeCl_2·4H_2O$ (Shantou Xilong Chemical Co., Ltd.) were used to synthesize the Fe_3O_4. $FeSO_4·7H_2O$ (Beijing Chemical Plant) and $Ti(SO_4)_2·12H_2O$ (Sinopharm Chemical Reagent Company) were used to synthesize the Fe–Ti oxide. The other chemicals used were ammonia (Beijing Modern East Fine Chemicals Co., Ltd.), anhydrous ethanol (Beijing Modern East Fine Chemicals Co., Ltd.), hydrochloric acid (Beijing Chemical Plant), cetyltrimethyl ammonium bromide (CTAB, Tianjin Bodi Chemical Co., Ltd.), and NaF (Beijing Modern East Fine Chemicals Co., Ltd.). All the chemicals were of analytical grade and were used without further purification.

2.2. Preparation of the Fe_3O_4 particles

The Fe_3O_4 particles were prepared by chemical precipitation method [23,30–34]. $FeCl_2·4H_2O$ and $FeCl_3·6H_2O$ were dissolved in ethanol to form a mixed solution with a total molar concentration of 0.3 M. The molar ratio of Fe^{2+} to Fe^{3+} was 5:1. A small amount of cetyltrimethyl ammonium bromide (CTAB) was added into the solution as a dispersant. The vessel was put in a water bath at 30 °C. 0.6 M ammonia solution was slowly titrated into the mixed solution under agitation until the pH reached 9.0. Agitation was continued for 5 min to complete the reaction. The slurry was aged for 3 h in the water bath at 50 °C. The precipitates were collected by a magnet and washed three times with deionized water. The Fe_3O_4 particles were kept in deionized water until used.

2.3. Preparation of magnetic composite nano-adsorbents

$FeSO_4·7H_2O$ and $Ti(SO_4)_2$ were dissolved in deionized water with Fe^{2+} and Ti^{4+} concentrations that were both 0.3 M. The mixed solution and 12.5% ammonia were simultaneously added dropwise into 10 g/L Fe_3O_4 suspension under agitation. The pH was kept at 4 ± 0.2 during the titration. The precipitates were collected using a magnet and washed three times with deionized water. The composite particles were kept in deionized water until the adsorption experiment. Part of the composite particles was dried at 80 °C for 12 h for further characterization.

2.4. Adsorbent characterization

A high-resolution transmission electron microscopy (HRTEM, JEM-2011, JEOL Co., Japan) was used to examine the morphology and microscopic structure of the adsorbents. The adsorbent crystal structure was examined by X-ray diffraction analysis (XRD, D8-Advance, Brucker, Germany) over a range of 10–90° (based on 2θ) with Cu Kα radiation at a scan speed of 5°/min. The magnetic properties of the adsorbents were analyzed by a vibrating sample magnetometer (VSM). The specific surface area of the adsorbents was measured by a nitrogen adsorption apparatus (Autosorb-iQ2-C, Quantachrome Instruments, USA). Surface elemental compositions of the particles at different stages of the coating process were determined by X-ray photoelectron spectroscopy (XPS, ESCALAB 250Xi, Thermo Fisher, USA) with a monochromic Al Kα radiation source (1486.6 eV). The binding energies were calibrated by the C1s peak at 284.8 eV. The elemental compositions of the particles and adsorbent residues were determined with inductively coupled plasma atomic emission spectroscopy (ICP, Vista-MPX, VARIAN, USA).

2.5. Adsorption studies

Adsorption properties were determined by batch adsorption experiments. A fluoride solution with a concentration of C_0 (mg/L) was prepared by dissolving NaF in deionized water. An adsorbent dose of W (g/L) was added into a conical flask containing 100 mL fluoride solution. The flask was shaken on a thermostat shaker at 180 rpm and 25 °C. In order to ensure adsorption equilibrium, the adsorption time was set for 12 h. The concentration of residual fluoride in the solution, C_e, was measured with a fluoride selective electrode connected to an ion meter (PXS-450, Shanghai Kang-Yi Instruments Co., LTD, China) using the method in GB/T 13083-2002. The equilibrium adsorption capacity of the adsorbent, Q_e, was calculated as

$$Q_e = (C_0 - C_e)/W \tag{1}$$

The adsorption capacity per unit mass of Fe–Ti oxide was calculated from the mass fraction of Fe–Ti oxide in the composite nano-adsorbent.

The adsorption kinetics was determined as follows. 1000 mL fluoride solution with a concentration of 10 mg/L and 1 g adsorbent were added into a conical flask. The flask was shaken on a thermostat shaker at 180 rpm and 25 °C. During the adsorption, solution samples with a volume of about 8 mL were taken from the flask at different times and their fluoride concentrations were measured. The adsorption amounts at different times were calculated using Eq. (1), and the adsorption rate was estimated from the slope of the plotted curve.

Fluoride solutions with concentrations of 5 mg/L to 200 mg/L were prepared and used for the batch adsorption experiment. The equilibrium adsorption amounts at different equilibrium concentrations were measured to give the adsorption isotherms, which were plotted and fitted to the Langmuir isotherm.

2.6. Separation of composite nano-adsorbents from the water solution

A 50 mm × 50 mm × 10 mm square Nd-Fe-B magnet (N30) was used to study the separation properties. The magnetic parameters were remanence = 1.08–1.12 T, coercivity = 9.8–10.5 kOe, and maximum energy product = 28–30 MGOe.

An adsorbent dose of W (g/L) was added into a conical flask containing 100 mL fluoride solution. The flask was put on the square magnet and kept for a set time, then a 10 mL sample was taken out
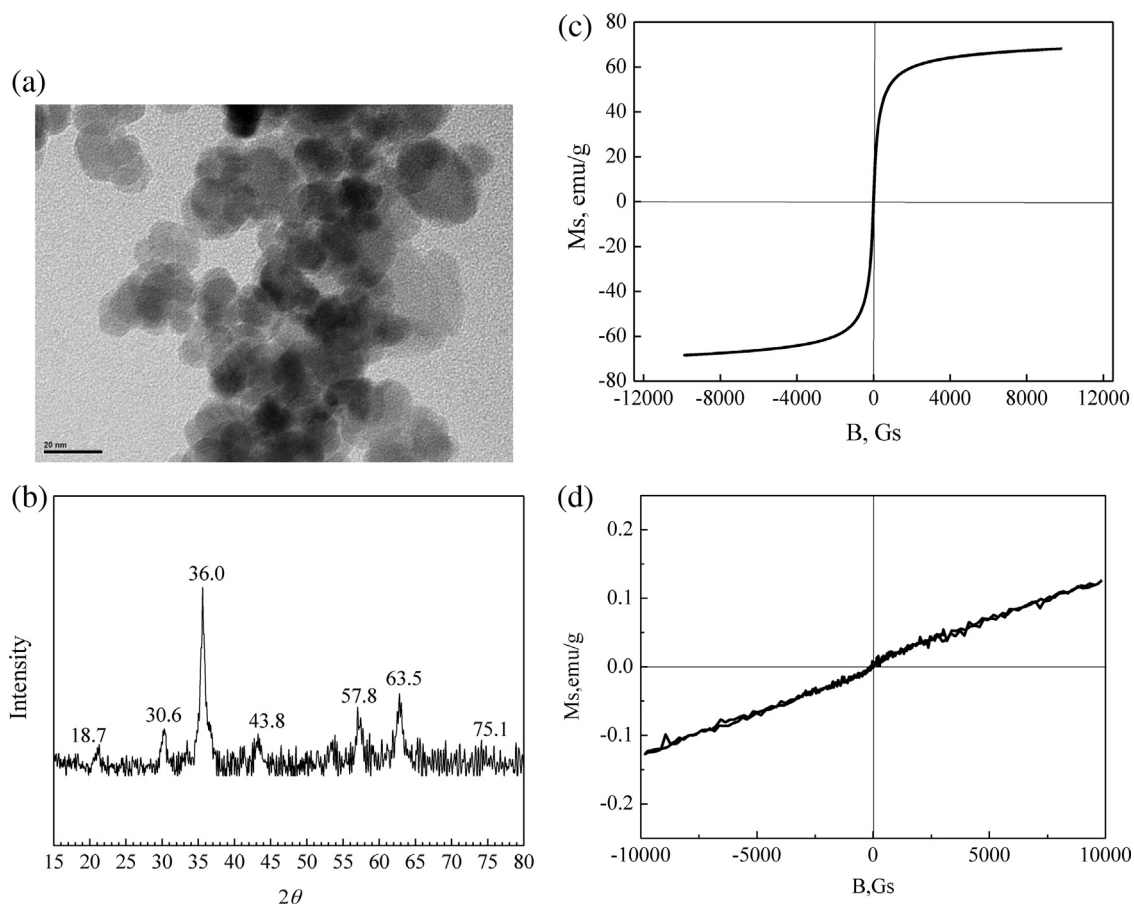
Fig. 1. TEM image, XRD spectrum and magnetic hysteresis loop of the magnetic Fe_3O_4 particles and non-magnetic Fe–Ti oxide. (a) TEM of the Fe_3O_4 particles. (b) XRD pattern of the Fe_3O_4 particles. (c) Magnetic hysteresis loop of the Fe_3O_4 particles. (d) Magnetic hysteresis loop of the Fe–Ti oxide.

slowly by a pipette from the supernatant and the solid residues in it were dissolved by excess sulfuric acid. The Fe and Ti residues in the sample, C_{Fe} and C_{Ti} (mg/L), were measured by ICP. The efficiency of the magnetic separation, R, was defined as

$$R = \left(1 - \frac{C_{Fe} + C_{Ti}}{1000 \times W}\right) \times 100\% \qquad (2)$$

A shorter separation time and lower R value indicated a higher separation efficiency.

3. Results and discussion

3.1. Magnetic properties of the composite nano-adsorbents

3.1.1. Magnetic core particle Fe₃O₄

The TEM image, XRD pattern and magnetic hysteresis loop of the prepared Fe_3O_4 particles are shown in Fig. 1. The Fe_3O_4 product comprised quasi-spherical particles with diameters of 10–20 nm. The characteristic XRD peaks at 18.7°, 30.6°, 36.0°, 43.8°, 57.8°, 63.5°, 75.1° confirmed that the main phase of the particles was crystalline Fe_3O_4. The coercive force and residual magnetization are both close to 0, indicating that the Fe_3O_4 was superparamagnetic. The saturation magnetization was 68.3 emu/g. For comparison, the hysteresis loop of the Fe–Ti oxide is also shown in Fig. 1(d). The Fe–Ti oxide is a paramagnetic material whose magnetic strength was negligible.

The coating of Fe–Ti oxide onto the Fe_3O_4 particle was performed in acidic solution (pH = 4). In order to determine a possible mass loss of Fe_3O_4 particles during the coating process, 0.0795 g Fe_3O_4 particles were dispersed in H_2SO_4 solution at pH = 4, shaken

for 2 h, and then re-collected with a magnet. The mass of collected particles was 0.0794 g, so the mass loss rate was 0.1%, indicating that the mass loss of Fe_3O_4 particles during the coating process was very small and can be ignored.

3.1.2. Magnetic composite nano-adsorbents

The coating amount in the composite nano-adsorbents can be adjusted by changing the amount of iron and titanium salt solution used in the coating process. The Ti/Fe mass ratio δ of the adsorbent was determined by ICP. A large δ value indicated a high coating amount. The XRD spectra of composite nano-adsorbents with different coating amounts are shown in Fig. 2. The XRD peaks of composite nano-adsorbents with different coating amounts were similar to the peaks of Fe_3O_4. This indicated that the Fe_3O_4 crystal structure was not changed in the coating process and the Fe–Ti oxide in the composite nano-adsorbent was confirmed to be amorphous.

The hysteresis loops of composite nano-adsorbents with different coating amounts are shown in Fig. 3. The composite nano-adsorbents have excellent superparamagnetic characteristics. The saturation magnetization decreased as the Fe–Ti oxide coating amount increased. This also confirmed that Fe–Ti oxide was non-magnetic, Fe_3O_4 was the only magnetic component in the composite nano-adsorbent, and the crystal structure of Fe_3O_4 was not changed by the coating process. Therefore, the magnetic properties of the composite nano-adsorbent was determined by the mass fraction of Fe_3O_4 [19].

Compared with the measured Ti/Fe mass ratio δ, the mass ratio of Fe–Ti oxide to Fe_3O_4, ϕ, is more useful for describing the coating amount, and this can be derived. Since the crystal structure of Fe_3O_4
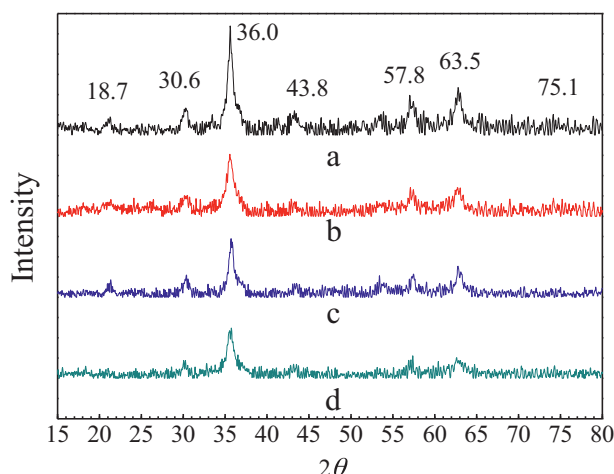
Fig. 2. XRD spectra of composite nano-adsorbents with different coating amounts. Ratio of Ti/Fe: (a) 0 (Fe$_3$O$_4$); (b) 0.78; (c) 1.10; (d) 1.49.

was not changed during the coating process and the mass loss of Fe$_3$O$_4$ can be ignored, the magnetic properties of the composite nano-adsorbent depended on the mass fraction of Fe$_3$O$_4$. Thus the saturation magnetization of Fe$_3$O$_4$ and composite nano-adsorbent, Ms_0 and Ms_1, have the relationship

$$Ms_1 = Ms_0 \times P \tag{3}$$

where P is the mass fraction of Fe$_3$O$_4$ in the composite nano-adsorbent,

$$P = \frac{M(\text{Fe}_3\text{O}_4)}{M(\text{Fe}_3\text{O}_4) + M(\text{Fe–Ti})} \tag{4}$$

Therefore, the mass ratio of Fe–Ti oxide to Fe$_3$O$_4$, ϕ, can be calculated from the magnetization,

$$\phi = \frac{M(\text{Fe–Ti})}{M(\text{Fe}_3\text{O}_4)} = \frac{Ms_0 - Ms_1}{Ms_1} \tag{5}$$

When the coating amount increased, the mass ratio ϕ of Fe–Ti oxide to Fe$_3$O$_4$ increased, as the corresponding mass ratio of Ti/Fe δ also increased. The chemical composition of the Fe–Ti oxide was determined to be Fe$_{0.12}$TiO$_{2.16}$. A linear relationship between ϕ^{-1} and δ^{-1} can be derived. ϕ was calculated from the saturation magnetization of the composite nano-adsorbent, and δ was measured by ICP. The curve of ϕ^{-1} versus δ^{-1} is shown in Fig. 4. Fig. 4 shows a linear correlation R^2 of 0.9998 for the two sets of data, that is, the

Fig. 4. Plot of ϕ^{-1} versus δ^{-1} (ϕ = Fe–Ti/Fe$_3$O$_4$, δ = Ti/Fe in mass).

composite nano-adsorbent composition calculated from saturation magnetization and that measured by ICP were in good agreement. This also indicated that the Fe$_3$O$_4$ core in the composite nano-adsorbent has the same magnetic properties as pure Fe$_3$O$_4$, and the magnetization of the composite nano-adsorbent was entirely due to the Fe$_3$O$_4$ core. For the composite nano-adsorbent with δ = 1.10, i.e., ϕ = 2.72, the saturation magnetization was 18.4 emu/g, which was a high value when compared with those in literature reports [19,20].

3.2. Core–shell structure of the composite nano-adsorbent

The greatest limitation for the fluoride adsorption using nano-adsorbents is the solid–liquid separation. A core–shell structure with magnetic Fe$_3$O$_4$ core and Fe–Ti adsorbent shell is the ideal structure to ensure a complete and efficient separation in a magnetic field.

The TEM morphology of the composite nano-adsorbent is shown in Fig. 5. As shown in Fig. 5(b), the composite nano-adsorbent had a core–shell structure. The core of the particle showed the diffraction fringes of the Fe$_3$O$_4$ crystal structure (marked in circle), while the coating layer was amorphous. The average thickness t_ϕ of the coating shell can be calculated,

$$t_\phi = 0.5d \times \left(\sqrt[3]{1 + \frac{\rho_c}{\rho_s}\phi} - 1 \right) \tag{6}$$

where d was the average diameter of the Fe$_3$O$_4$ core, and ρ_c, ρ_s were the densities of Fe$_3$O$_4$ core and Fe–Ti shell, which were 5.18 g/cm^3 and 4.34 g/cm^3, respectively. For the composite nano-adsorbent with ϕ = 2.72 and the average diameter of the Fe$_3$O$_4$ core at about 15 nm (average value from TEM images), the average thickness of the shell was calculated to be 4.7 nm, which was in close agreement with the shell thickness observed in Fig. 5(b). Therefore, it is inferred that most of the composite nano-adsorbent particles had a core–shell structure with Fe$_3$O$_4$ particle core and Fe–Ti oxide shell.

In order to further verify the core–shell structure of the composite nano-adsorbent, the surface compositions for the composite adsorbents using a core–shell structure model or a physical mixture model was calculated and compared with the XPS detected values, for different macroscopic compositions ϕ (the mass ratio of Fe–Ti oxide to Fe$_3$O$_4$). The XPS spectra for different ϕ showed similar characteristics except for the small difference of Ti and Fe peak strengths. Fig. 6 showed the XPS spectrum for ϕ = 0.63. The atomic ratios of Ti, Fe, O, C were calculated from the XPS spectra and presented in Table 2, from which the Ti/Fe mass ratios were
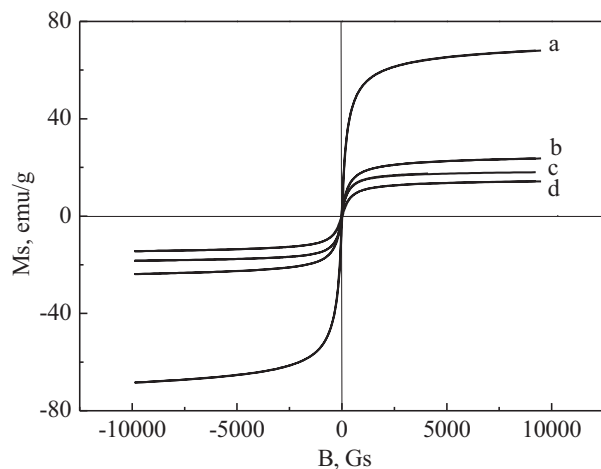

Fig. 3. Magnetic hysteresis loops of composite nano-adsorbents with different coating amounts. Ratio of Ti/Fe: (a) 0 (Fe$_3$O$_4$); (b) 0.78; (c) 1.10; (d) 1.49.
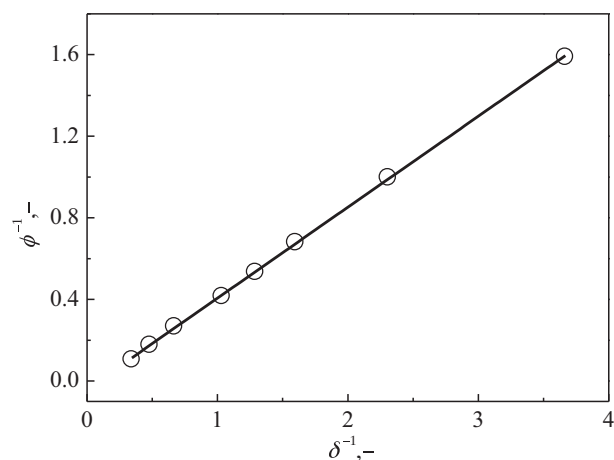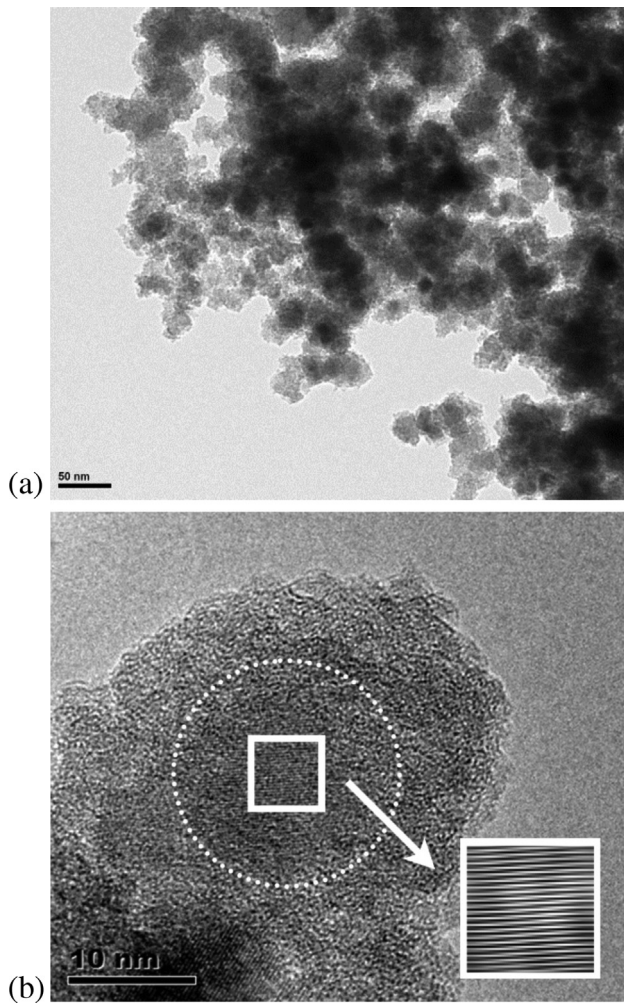
obtained and taken as the surface compositions for the composite adsorbents.

The probing depth of XPS could be calculated through the empirical formula of Seah and Dench [35],

$$d_{XPS} = a \times (2170E^{-2} + 0.72(aE)^{0.5}) \tag{7}$$

$$a^3 = \frac{M}{\rho n N} \tag{8}$$

where d_{XPS} was the probing depth of XPS, a was the monolayer thickness of the molecular, E was the electron energy, M was the molecular weight, ρ was the density, n was the atom number, N was the Avogadro constant. The densities of Fe_3O_4 and Fe–Ti oxide particles were 5.18 g/cm^3 and 4.34 g/cm^3, respectively. The molecular formula of Fe–Ti oxide determined through ICP was $Fe_{0.12}TiO_{2.16}$. The monolayer thickness of Fe_3O_4 and Fe–Ti were calculated to be 0.21 nm and 0.23 nm, respectively. For the composite nano-adsorbents, the average thickness a of Fe_3O_4 and Fe–Ti oxide was taken as 0.22 nm. According to the kinetic energy of electrons from Fe2p (767 eV) and Ti2p (1017 eV), the calculated probing depths of Fe and Ti were 2.1 nm and 2.4 nm respectively. Therefore, the sample surface of 2.4 nm could be detected by XPS. So 2.4 nm was chosen as the probing depth in the calculation.

The surface compositions for both models were calculated,

$$\delta_{cal} = \frac{m_{Fe-Ti} \times W_{Ti, Fe-Ti}}{m_{Fe-Ti} \times W_{Fe, Fe-Ti} + m_{Fe_3O_4} \times W_{Fe, Fe_3O_4}} \tag{9}$$

$W_{Ti,Fe-Ti}$ and $W_{Fe,Fe-Ti}$ were the mass ratios of Ti and Fe in Fe–Ti oxide, and W_{Fe,Fe_3O_4} was the mass ratio of Fe in Fe_3O_4, which were 0.54, 0.08 and 0.72 respectively. m_{Fe-Ti} and $m_{Fe_3O_4}$ were the probing mass of Fe–Ti oxide and Fe_3O_4 of the sample surface, depending on the structure model.

For a core–shell structure model, the detected surface contained the Fe–Ti shell and a thin layer of the inner Fe_3O_4 core. When Fe–Ti shell thickness $t_\phi < d_{XPS}$ (i.e. 2.4 nm), δ_{cal} would increase as t_ϕ increased. When $t_\phi > d_{XPS}$, the detected part was pure Fe–Ti, and δ_{cal} would remain constant. Then $m_{Fe-Ti}/m_{Fe_3O_4}$ was calculated,

$$\frac{m_{Fe-Ti}}{m_{Fe_3O_4}} = \frac{\rho_s \times [(d_{Fe_3O_4} + 2t_\phi)^3 - d_{Fe_3O_4}{}^3]}{\rho_c \times [d_{Fe_3O_4}{}^3 - (d_{Fe_3O_4} + 2t_\phi - 2d_{XPS})^3]}, \quad t_\phi < d_{XPS} \tag{10}$$

$$m_{Fe_3O_4} = 0 \quad \text{and} \quad \delta_{cal} = \frac{W_{Ti,Fe-Ti}}{W_{Fe,Fe-Ti}}, \quad t_\phi \geq d_{XPS} \tag{11}$$

The average diameters of the Fe_3O_4 particles, $d_{Fe_3O_4}$, was 15 nm. The Fe–Ti shell thickness t_ϕ was calculated from Eq. (6).

For a physical mixture model, the detected surface contained the outer layer of independent Fe_3O_4 and Fe–Ti particles, and δ_{cal} would increase as Fe–Ti mass fraction ϕ increased. Considering d_{XPS} = 2.4 nm, the average diameters of the Fe_3O_4 particles about 15 nm and the Fe–Ti particles about 4 nm[12], $m_{Fe-Ti}/m_{Fe_3O_4}$ was calculated,

$$\frac{m_{Fe-Ti}}{m_{Fe_3O_4}} = \phi \times \frac{d_{Fe_3O_4}{}^3}{d_{Fe_3O_4}{}^3 - (d_{Fe_3O_4} - 2d_{XPS})^3} \tag{12}$$

The detected surface compositions and the predicted compositions for the two models at ϕ = 0.63, 1.00, 1.87, 3.74 were presented in Fig. 7. It showed that the core–shell model compositions were in good agreement with the detected trend, while the physical mixture compositions showed a linear-like trend and was far below the detected compositions. The standard deviation for core–shell model was 0.30, while that for physical mixture model was 0.79, indicating the core–shell model was much closer to the composite adsorbent structure than the physical mixture model. It is also an evidence for the formation of core–shell structure.

Fig. 5. Core–shell structure of the composite nano-adsorbent (ϕ = 2.72). (a) Composite nano-adsorbent. (b) Core–shell structure.
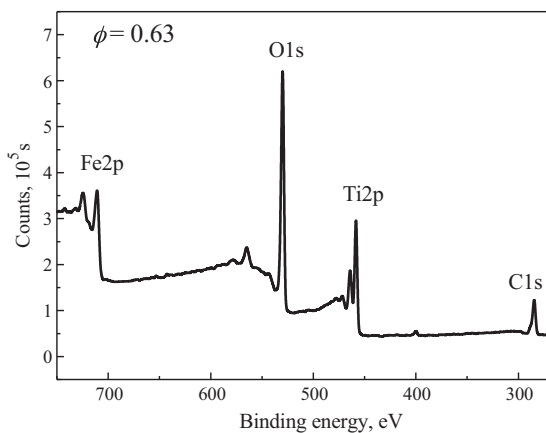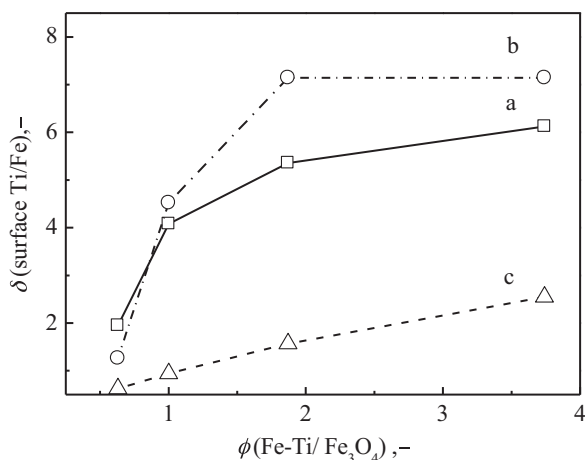

Fig. 6. The XRS spectrum of the composite nano-adsorbent (ϕ = 0.63).

Table 2
Surface compositions for different macroscopic compositions detected by XPS.

ϕ, Fe–Ti/Fe$_3$O$_4$ mass ratio	Atomic ratios, %				Ti/Fe mass ratio
	Ti	Fe	O	C	
0.63	14.1	6.2	39.6	40.1	1.95
1.00	16.2	3.4	35.4	45.0	4.08
1.87	17.9	2.8	32.6	46.7	5.36
3.74	18.8	2.6	32.3	46.3	6.12

Fig. 7. Compare between detected surface compositions and model predictions. (a) XPS detected surface compositions; (b) core–shell model calculation; (c) physical mixture model calculation.
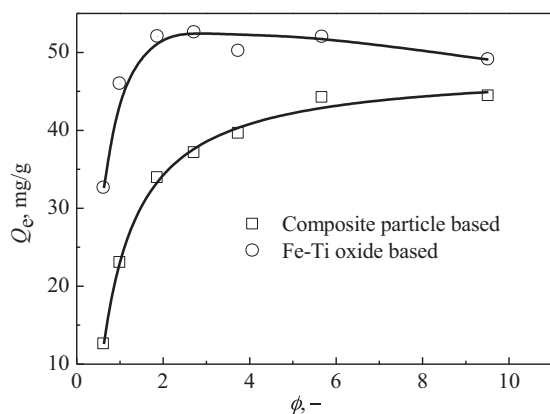

Fig. 8. Q_e of the composite nano-adsorbent versus ϕ.

In addition, the specific surface areas for the Fe_3O_4 particles and composite nano-adsorbents ($\phi = 2.72$) measured by nitrogen adsorption were 127.12 m^2/g and 115.32 m^2/g, respectively. This was consistent with that the specific surface area would decrease since the particle size was increased due to that the Fe_3O_4 particles were coated with the Fe–Ti oxide to form a core–shell structure.

3.3. Effects of coating amount on adsorption capacity

The adsorption capacities of Fe_3O_4, Fe–Ti oxide and composite nano-adsorbent were measured by batch adsorption experiments. The results were shown in Table 3. The adsorption capacity of the Fe_3O_4 particles was close to 0. The adsorption capacity of the composite nano-adsorbent, Q_e, was mainly due to the Fe–Ti oxide coated on the surface.

The fluoride adsorption capacities of the composite nano-adsorbents at different ϕ were measured. The results were shown in

Table 3
Q_e of Fe_3O_4, Fe–Ti oxide and composite nano-adsorbent.[a]

Sample	Fe_3O_4	Fe–Ti oxide	Composite nano-adsorbent
Q_e (mg/g)	0.30	43.18	37.13

[a] Adsorption conditions: initial fluoride concentration 50 mg/L; particle dose 1 g/L; adsorption time 12 h; shaker thermostat at 25 °C; shaking rate 180 rpm. Composite nano-adsorbent at $\phi = 2.72$.

Table 4
Fitted Langmuir parameters of the composite nano-adsorbent.

Parameters	Q_{max} (mg/g)	b (L/mg)	R^2 (−)
Value	41.84	0.23	0.9983

Fig. 8. As ϕ increased, the adsorption capacity per mass of composite nano-adsorbent increased, then the increase slowed gradually until a final stabilized value was reached. The adsorption capacity Q_e based on the mass of Fe–Ti increased to a maximum at ϕ 2.72, and then decreased. This was because when the coating layer had increased to a certain thickness, the innermost Fe–Ti oxide does not contribute to the adsorption. If the Fe_3O_4 particles were only mixed physically with the Fe–Ti oxide, the adsorption capacity should increase linearly with the Fe–Ti oxide content, and the capacity per mass of Fe–Ti oxide should remain unchanged, which was inconsistent with Fig. 8. Therefore, Fig. 8 also confirmed the core–shell structure of the Fe_3O_4 particles and Fe–Ti oxide in the composite nano-adsorbents.

As shown in Fig. 8, the adsorbent capacity per mass of Fe–Ti oxide reached a maximum value at $\phi = 2.72$. Therefore, ϕ was set to 2.72 in the preparation of the composite nano-adsorbent in the following experiments. (Initial fluoride concentration 50 mg/L; particle dose 1 g/L; adsorption time 12 h, shaker thermostat 25 °C, shaking rate 180 rpm.)

3.4. Adsorption properties of the composite nano-adsorbent

The adsorption equilibrium data were fitted to the Langmuir isotherm equation [36]:

$$Q_e = \frac{Q_{max} b C_e}{1 + b C_e} \tag{13}$$

where Q_{max} is the maximum monolayer adsorption capacity (mg/g), and b is the Langmuir constant (L/mg), which expresses the affinity of the adsorbate for the adsorption sites. The model assumes that all the adsorption sites of the adsorbent have the same binding energy, and the adsorption results in a monolayer.

In order to make it easier to get the parameters Q_{max} and b, Eq. (13) was transformed into a linear form [36],

$$\frac{C_e}{Q_e} = \frac{1}{Q_{max}} \times C_e + \frac{1}{Q_{max} b} \tag{14}$$

Q_{max} and b were obtained from the slope and intercept of the linear fit of C_e/Q_e and C_e. The fitted results were shown in Table 4.
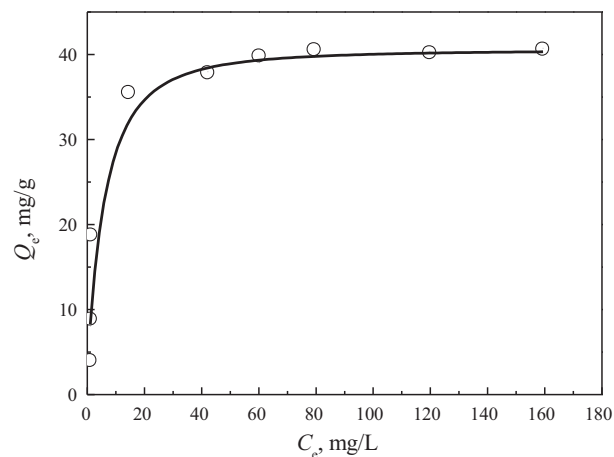

Fig. 9. Experimental data and fitted adsorption isotherm (adsorbent dose 1 g/L; adsorption time 12 h, shaker thermostat 25 °C, shaking rate 180 rpm).
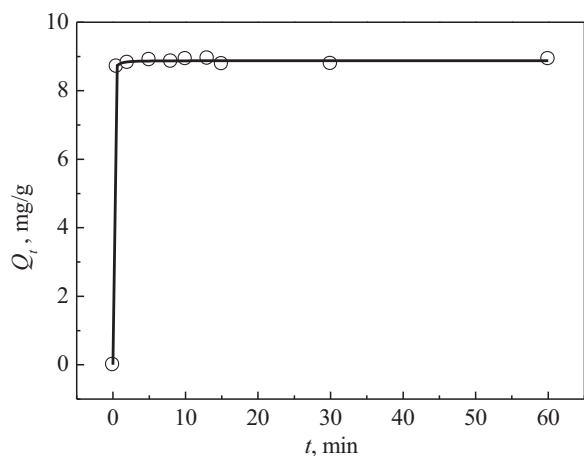
Fig. 10. Adsorption amounts versus adsorption time (initial fluoride concentration 10 mg/L; adsorbent dose 1 g/L; adsorption time 12 h, shaker thermostat 25 °C, shaking rate 180 rpm).

Table 5
Magnetic separation results of the composite adsorbent from the water solution (adsorbent dose 1 g/L).

Time (min)	Fe (mg/L)	Ti (mg/L)	Separation efficiency, %
1	6.82	4.62	98.86
3	4.84	2.64	99.25
5	5.06	2.42	99.25
7	5.06	2.42	99.25
10	4.40	2.20	99.34

The experimental data and fitted curve of the adsorption isotherms were shown in Fig. 9, which showed an excellent fit. The fitted Langmuir saturation adsorption capacity was 41.84 mg/g, and the Langmuir adsorption capacity per mass of Fe–Ti oxide was 57.22 mg/g.

The adsorption kinetics data were shown in Fig. 10. The adsorption reached equilibrium within 2 min, indicating that the composite nano-adsorbent had a high adsorption rate. That is, the composite nano-adsorbent not only has a high adsorption capacity, but also has a fast absorption rate, which makes it an ideal adsorbent for fluoride removal.

3.5. Separation of the composite nano-adsorbent from the water solution

It was shown in Table 5 that over 99% of the composite nano-adsorbents was separated within 3 min by the magnet. An increased separation time did not increase the separation efficiency significantly, indicating that under the applied magnetic field, the separation basically reached equilibrium within 3 min. To further improve the separation efficiency, the strength of the magnet has to be increased.

In summary, it was shown that the composite nano-adsorbent can be separated efficiently in a short time with an applied magnetic field, that is, it had an excellent solid–liquid separation performance. Therefore, the composite nano-adsorbent can be used in a fluidized system to give high absorption capacity, fast adsorption rate, and efficient solid–liquid separation.

4. Conclusion

A novel composite nano-adsorbent with a core–shell structure for fluoride removal from drinking water was prepared by coating a high adsorption capacity Fe–Ti oxide layer onto superparamagnetic

Fe_3O_4 particles. At a mass ratio of Fe–Ti oxide to Fe_3O_4 core of 2.72, the adsorption capacity per unit mass of Fe–Ti oxide reached a maximum of 57.22 mg/g, which corresponded the highest utilization efficiency of the adsorption capacity of Fe–Ti oxide. The adsorption isotherms were well fitted with the Langmuir model, and adsorption reached equilibrium within 2 min. The saturation magnetization was 18.4 emu/g, which ensured rapid separation of the composite nano-adsorbent from the water solution by an external magnet. The magnetic composite nano-adsorbent can be used in a fluidized system for fluoride adsorption to give high absorption capacity, fast adsorption rate, and efficient solid–liquid separation.

References

[1] S. Ayoob, A.K. Gupta, Fluoride in drinking water: a review on the status and stress effects, Crit. Rev. Environ. Sci. Technol. 36 (2006) 433–487.
[2] A. Ghosh, K. Mukherjee, S.K. Ghosh, B. Saha, Sources and toxicity of fluoride in the environment, Res. Chem. Intermed. 39 (2013) 2881–2915.
[3] F. Bruce, Guidelines for drinking-water quality. Vol. 2. Health criteria and other supporting information – WHO, J. R. Soc. Health 106 (1986) 111.
[4] M. Mohapatra, S. Anand, B.K. Mishra, D.E. Giles, P. Singh, Review of fluoride removal from drinking water, J. Environ. Manag. 91 (2009) 67–77.
[5] S. Meenakshi, R.C. Maheshwari, Fluoride in drinking water and its removal, J. Hazard. Mater. 137 (2006) 456–463.
[6] A. Bhatnagar, E. Kumar, M. Sillanpää, Fluoride removal from water by adsorption – a review, Chem. Eng. J. 171 (2011) 811–840.
[7] M.G. Sujana, A. Mishra, B.C. Acharya, Hydrous ferric oxide doped alginate beads for fluoride removal: adsorption kinetics and equilibrium studies, Appl. Surf. Sci. 270 (2013) 767–776.
[8] Z. Shengyu, L. Ying, L. Xueyu, S. Xiaosi, Z. Yuling, Removal of fluoride from groundwater by adsorption onto La(III)–Al(III) loaded scoria adsorbent, Appl. Surf. Sci. 303 (2014) 1–5.
[9] S. Mulyati, R. Takagi, A. Fujii, Y. Ohmukai, H. Matsuyama, Simultaneous improvement of the monovalent anion selectivity and antifouling properties of an anion exchange membrane in an electrodialysis process, using polyelectrolyte multilayer deposition, J. Membr. Sci. 431 (2013) 113–120.
[10] M.F. Chang, J.C. Liu, Precipitation removal of fluoride from semiconductor wastewater, J. Environ. Eng. ASCE 133 (2007) 419–425.
[11] D. Ghosh, M.K. Sinha, M.K. Purkait, A comparative analysis of low-cost ceramic membrane preparation for effective fluoride removal using hybrid technique, Desalination 327 (2013) 2–13.
[12] R.S. Keri, K.M. Hosamani, H.R.S. Reddy, S.K. Nataraj, T.M. Aminabhavi, Application of the electrodialytic pilot plant for fluoride removal, J. Water Chem. Technol. 33 (2011) 293–300.
[13] L. Chen, B.Y. He, S. He, T.J. Wang, C.L. Su, Y. Jin, Fe–Ti oxide nano-adsorbent synthesized by co-precipitation for fluoride removal from drinking water and its adsorption mechanism, Powder Technol. 227 (2012) 3–8.
[14] L. Chen, S. He, B.Y. He, T.J. Wang, C.L. Su, C. Zhang, Y. Jin, Synthesis of iron-doped titanium oxide nano-adsorbent and its adsorption characteristics for fluoride in drinking water, Ind. Eng. Chem. Res. 51 (2012) 13150–13156.
[15] K. Biswas, S.K. Saha, U.C. Ghosh, Adsorption of fluoride from aqueous solution by a synthetic iron(III)–aluminum(III) mixed oxide, Ind. Eng. Chem. Res. 46 (2007) 5346–5356.
[16] K. Biswas, D. Bandhoyapadhyay, U.C. Ghosh, Adsorption kinetics of fluoride on iron(III)–zirconium(IV) hybrid oxide, Adsorption 13 (2007) 83–94.
[17] K. Biswas, K. Gupta, U.C. Ghosh, Adsorption of fluoride by hydrous iron(III)–tin(IV) bimetal mixed oxide from the aqueous solutions, Chem. Eng. J. 149 (2009) 196–206.
[18] K. Biswas, S. Debnath, U.C. Ghosh, Physicochemical aspects on fluoride adsorption for removal from water by synthetic hydrous iron(III)–chromium(III) mixed oxide, Sep. Sci. Technol. 45 (2010) 472–485.
[19] C.-F. Chang, P.-H. Lin, W. Höll, Aluminum-type superparamagnetic adsorbents: synthesis and application on fluoride removal, Coll. Surf. A: Physicochem. Eng. Asp. 280 (2006) 194–202.
[20] X. Zhao, J. Wang, F. Wu, T. Wang, Y. Cai, Y. Shi, G. Jiang, Removal of fluoride from aqueous media by Fe_3O_4@Al(OH)$_3$ magnetic nano-particles, J. Hazard. Mater. 173 (2010) 102–109.
[21] Z. Samra, S. Ahmad, S. Javeid, N. Dar, M. Aslam, I. Gull, M. Ahmad, Anticancer medicines (doxorubicin and methotrexate) conjugated with magnetic nano-particles for targeting drug delivery through iron, Prep. Biochem. Biotechnol. 43 (2013) 781–797.

[22] D. Horak, M. Babic, H. Mackova, M.J. Benes, Preparation and properties of magnetic nano- and microsized particles for biological and environmental separations, J. Sep. Sci. 30 (2007) 1751–1772.

[23] J.H. Ji, P.H. Zeng, S.F. Ji, W. Yang, H.F. Liu, Y.Y. Li, Catalytic activity of core–shell structured Cu/Fe$_3$O$_4$@SiO$_2$ microsphere catalysts, Catal. Today 158 (2010) 305–309.

[24] D. Makovec, M. Sajko, A. Seisnik, M. Drofenik, Magnetically recoverable photocatalytic nanocomposite particles for water treatment, Mater. Chem. Phys. 129 (2011) 83–89.

[25] G. Zhang, J. Qu, H. Liu, R. Liu, R. Wu, Magnetic adsorbents: activated carbon/iron oxide composites for AO7 removal from aqueous system, Acta Sci. Circumst. (2006) 1763–1768.

[26] A.-F. Ngomsik, A. Bee, D. Talbot, G. Cote, Magnetic solid–liquid extraction of Eu(III), La(III), Ni(II) and Co(II) with maghemite nano-particles, Sep. Purif. Technol. 86 (2012) 1–8.

[27] T. Poursaberi, M. Hassanisadi, K. Torkestani, M. Zare, Development of zirconium (IV)–metalloporphyrin grafted Fe$_3$O$_4$ nano-particles for efficient fluoride removal, Chem. Eng. J. 189–190 (2012) 117–125.

[28] S. Asuha, Y.M. Zhao, S. Zhao, W. Deligeer, Synthesis of mesoporous maghemite with high surface area and its adsorptiveproperties, Solid State Sci. 14 (2012) 833–839.

[29] Q. Chang, L. Zhu, Z. Luo, M. Lei, S. Zhang, H. Tang, Sono-assisted preparation of magnetic magnesium–aluminum layered doublehydroxides and their application for removing fluoride, Ultrason. Sonochem. 18 (2011) 553–561.

[30] S. Laurent, D.F. Marc Port, A. Roch, C. Robic, L.V. Elst, R.N. Muller, Magnetic iron oxide nano-particles: synthesis, stabilization, vectorization, physicochemical characterizations, and biological applications, Chem. Rev. 108 (2008) 46.

[31] Y. Junejo, A. Baykal, H. Sozeri, Simple hydrothermal synthesis of Fe$_3$O$_4$-PEG nanocomposite, Cent. Eur. J. Chem. 11 (2013) 1527–1532.

[32] Y. Yin, C.J. Liu, B.X. Wang, S.S. Yu, K.Z. Chen, The synthesis and properties of bifunctional and intelligent Fe$_3$O$_4$@titanium oxide core/shell nano-particles, Dalton Trans. 42 (2013) 7233–7240.

[33] Z. Lei, X. Pang, N. Li, L. Lin, Y. Li, A novel two-step modifying process for preparation of chitosan-coated Fe$_3$O$_4$/SiO$_2$ microspheres, J. Mater. Process. Technol. 209 (2009) 3218–3225.

[34] Y. Lu, Y. Yin, B.T. Mayers, Y. Xia, Modifying the surface properties of superparamagnetic iron oxide nano-particles through a sol–gel approach, Nano Lett. 2 (2002) 183–186.

[35] M.P. Seah, W.A. Dench, Quantitative electron spectroscopy of surface: a stantard data base for electron inelastic mean free paths in solids, Surf. Interf. Anal. 1 (1979) 2.

[36] S. Meski, H. Khireddine, S. Ziani, S. Rengaraj, M. Sillanp, Comparative study on theremoval of zinc(II) by bovine bone, billy goat bone and synthetic hydroxyapatite, Desalin. Water Treat. 16 (2010) 271–281.